Chapter 2
The Ising Spin Glass in a Field

This chapter is dedicated to the search of a would-be phase transition in a three-dimensional spin glass. The discussion will focus entirely on the analysis of the data and on the results. We want to stress, in this context, that the equilibrium MC simulations performed in [BJ14a] required huge numerical efforts. On the one hand, lower temperatures drastically increased thermalization times; on the other hand, the significance of the results depends upon the size of the systems we are able to simulate.

The problem of enhancing the reach of our simulations is faced by resorting to advanced algorithms and techniques, such as PT[1] and MSC,[2] but that is still not enough. It would not have been possible to attain the results published in [BJ14a] with the mere use of ordinary computational resources. We drew upon (HPC) on one side by making use of the JANUS dedicated computer to simulate the largest lattices, and on the other by simulating the smaller systems on a large CPU cluster, *Memento*.

2.1 The de Almeida-Thouless Line in Three Dimensions

In Sect. 1.1.2 we explained that the nature of the SG phase in three dimensions it is still matter of debate. The two dominant theories are the droplet picture and the RSB scenario, and they have different predictions on the presence of a SG phase in a field. In the droplet picture even the smallest applied magnetic field destroys the SG phase, while in the RSB scenario there is a DAT line $h_c(T)$ that separates the SG from the paramagnetic phase.

A rather obvious way out would be the experimental study of spin glasses in a field. Unfortunately, opposing indications have been gleaned over the existence of a phase transition [Jön05, Pet99, Pet02, Tab10].

[1] A short discussion on PT is given in Appendix A.1.

[2] In Appendix B.3 we describe how MSC was implemented in the analysis stage. Multi-spin coding MC in the simulations [Seo13] follows roughly the same principles than in the analyses.

M. Baity Jesi, *Spin Glasses*, Springer Theses, DOI 10.1007/978-3-319-41231-3_2

The RG approach to this problem also provides conflicting results. No FPs were found by enforcing that the number of replicas of the replicated field theory be zero [Bra80b]. However, FPs were found relaxing this condition and using the most general Hamiltonian [Tem02]. Reasoning along this line, in [Tem08] (see also [Par12b]) the DAT line was computed for d slightly below the upper critical dimension $d_u = 6$ (the upper critical dimension remains 6 when an external magnetic field is applied).

Equilibrium numerical simulations offer an alternative approach, which has already been effective in establishing that a phase transition does occur at zero field in the $d = 3$ Edwards–Anderson model [Pal99a, Bal00] (in agreement with experiments [Gun91]). The same strategy has been followed for $h > 0$, with negative results [You04, Jör08b]. Yet, this cannot be the whole story: Recent work in $d = 4$, hence below d_u, using a non-standard finite-size scaling method has found clear evidence for a DAT line [Bn12a]. Furthermore, one may try to interpolate between $d = 3$ and $d = 4$ by tuning long-range interactions in $d = 1$ chains [Kot83, Leu08]. This approach suggests that a DAT might be present in $d = 4$, but not in $d = 3$ [Lar13] (yet, see the criticism in [Leu13]).

The problem being still open, in [BJ14b] we undertook a dynamical study of the 3-dimensional EA spin glass with the JANUS dedicated computer [Bel06, Bel08a, Bel09b, AB10a, Bn11, BJ12]. We studied very large lattices ($L^3 = 80^3$), in wide time scales (from an equivalent of $\sim$1 ps to $\sim$0.01 s), and gathered both equilibrium and non-equilibrium data. We focused on the increase of relaxation times and found a would-be dynamical transition, but at a suspiciously high temperature. A subsequent examination of the correlation length found a growth faster than predicted by the droplet theory, and slower than what RSB would expect. We also examined the problem from a supercooled liquid point of view [Deb97, Deb01, Cav09, Cas05, Kir87, Kir89], motivated by the equivalence of universality classes between spin and structural glasses [Moo02, Ful13]. At any rate, the study of the possible critical divergence of the correlation length allowed us to give upper bounds $T^{\mathrm{up}}(h)$ to the possible transition line for the studied fields.

The impossibility to get concluding evidence in [BJ14b], may be due to the fact that we did not reach low enough temperatures (our simulations fell out of equilibrium at temperatures T significantly higher than $T^{\mathrm{up}}(h)$). In any case, a study of the equilibrium properties of the model is mandatory if one wants to understand the nature of the thermodynamic phases of the three-dimensional EA spin glass in a field.

In this dissertation we will not talk about the aforementioned out-of-equilibrium results [BJ14b]. We will instead focus on the result of equilibrium simulations performed on JANUS, using lattices up to $L = 32$ [BJ14a].[3] For further reference we recall that $T^{\mathrm{up}}(h = 0.1) = 0.8$ and $T^{\mathrm{up}}(h = 0.2) = T^{\mathrm{up}}(h = 0.3) = 0.5$. Analogously to what has been already found in mean-field spin glasses on the DAT line, we find extreme fluctuations in the model's behavior [Par12a]. We will propose a

[3] In [BJ14b] we studied a bimodal field, while in the work we present here h is constant. Notwithstanding, we will make comparisons with the bounds $T^{\mathrm{up}}(h)$ by matching $\overline{h^2}$ in both models.

method to tame these fluctuations, and we will find out that, although the average behavior does not show any sign of a phase transition, this is not true for the medians of our observables, where we have indications of a possible phase transition at a temperature $T_c \lesssim T^{up}(h)$.

2.2 Model and Simulations

2.2.1 The 3d Edwards–Anderson Model in a Field

We consider a $3d$ cubic lattice of linear size L with periodic boundary conditions. In each of the $N = L^3$ vertices of the lattice there is an Ising spin $s_{\boldsymbol{x}} = \pm 1$. The spins interact uniquely with their nearest neighbors and with an external magnetic field h. The Hamiltonian is

$$\mathcal{H}_h = -\frac{1}{2} \sum_{|\boldsymbol{x}-\boldsymbol{y}|=1} J_{\boldsymbol{x}\boldsymbol{y}} s_{\boldsymbol{x}} s_{\boldsymbol{y}} - h \sum_{\boldsymbol{x}} s_{\boldsymbol{x}}, \tag{2.1}$$

where the couplings $J_{\boldsymbol{x}\boldsymbol{y}}$, which are constant during each simulation, take the values ± 1 with equal probability (quenched disorder). As already stated in Sect. 1.2.4, a given instance of the bonds $J_{\boldsymbol{x}\boldsymbol{y}}$ and of the intensity of the magnetic field h define a *sample*. We will consider real *replicas* of each sample, i.e., systems with identical couplings $J_{\boldsymbol{x}\boldsymbol{y}}$ and field h, but independent evolutions (for a recent discussion see [Bel09a, AB10a]). In this work we will use 4 replicas per sample.

2.2.2 The Simulations

For all our simulations we made use of PT.[4] The whole procedure was very similar to the one in [Bn12a].

The smaller lattices ($L = 6, 8, 12$) were simulated with MSC (C code with words of 128 bits, by means of streaming extensions) [New99, Bn12a, Seo13] on the *Memento* CPU cluster at BIFI. See details on MSC in Appendix B.3. The larger samples ($L = 16, 24, 32$) were simulated on the JANUS computer [Bel06, BJ12].

An EMCS consisted in 1 PT exchange every 10 Metropolis steps for the MSC samples, and 1 PT every 10 (HB) for the samples simulated on JANUS. Table 2.1 shows the relevant parameters of the simulations. The temperatures were equally spaced between T_{min} and T_{max}. The intensities of the external magnetic field we chose are $h = 0.05, 0.1, 0.2$ and 0.4.

[4] See the short note in Appendix A.1.

Table 2.1 Parameters of the simulations

h	L	N_{samples}	$N_{\text{EMCS}}^{\text{min}}$	f_{max}	N_{τ}^{min}	N_{T}	T_{min}	T_{max}
0.05	6	25600	1.6×10^6	1	40.0	14	0.5	1.8
0.05	8	25600	3.2×10^6	16	40.0	14	0.5	1.8
0.05	12	25600	3.2×10^6	16	15.6	12	0.7	1.8
0.05	16	12800	1.28×10^7	128	20.1	24	0.6	1.75
0.05	24	6400	1.28×10^7	110	16.0	20	0.78	1.54
0.05	32	2400	6.4×10^7	256	14.3	30	0.805128	1.54872
0.1	6	25600	1.6×10^6	4	40.0	14	0.5	1.8
0.1	8	25600	3.2×10^6	16	40.0	14	0.5	1.8
0.1	12	25600	3.2×10^6	16	14.4	12	0.7	1.8
0.1	16	12800	1.28×10^7	256	27.9	24	0.6	1.75
0.1	24	3200	1.28×10^7	4097	14.3	24	0.66	1.58
0.1	32	1600	6.4×10^7	533	14.4	30	0.805128	1.54872
0.2	6	25600	1.6×10^6	1	40.0	14	0.5	1.8
0.2	8	25600	3.2×10^6	16	40.0	14	0.5	1.8
0.2	12	25600	3.2×10^6	64	25.4	12	0.7	1.8
0.2	16	12800	1.28×10^7	256	18.4	24	0.6	1.75
0.2	24	3200	1.28×10^7	512	16.1	24	0.66	1.58
0.2	32	1600	1.6×10^7	513	16.0	30	0.805128	1.54872
0.4	6	25600	1.6×10^6	1	40.0	14	0.5	1.8
0.4	8	25600	3.2×10^6	4	30.7	14	0.5	1.8
0.4	12	25600	3.2×10^6	16	14.1	12	0.7	1.8
0.4	16	3200	1.28×10^7	32	20.1	24	0.6	1.75
0.4	24	800	1.28×10^7	29	16.1	24	0.66	1.58
0.4	32	800	3.2×10^6	16	16.4	30	0.805128	1.54872

We report the magnetic field h, the lattice linear size L, the number of simulated samples N_{samples}, and the basic length of a simulation in EMCS $N_{\text{EMCS}}^{\text{min}}$. In each simulation we measured the exponential correlation time τ of the PT random walk in temperatures. When τ was too large to meet our thermalization requirements, we extended the length of each simulation by an extension factor f. We denote with f_{max} the greatest extension factor. We also give the minimum length of a simulation N_{τ}^{min} in units of τ. In all cases we imposed $N_{\tau}^{\text{min}} > 14$. Finally, we give the number of temperatures N_T we used for the PT, and the minimum and maximum temperatures T_{min} and T_{max}

To check whether the samples were thermalized we measured the exponential autocorrelation time of the PT random walk in temperatures τ [Fer09b, AB10a, Yll11, Bn12a]. We required the simulations to last at least 14τ. To do so without consuming computing time on already thermalized lattices, we assigned a minimum number of EMCS, $N_{\text{EMCS}}^{\text{min}}$, for all the samples, and extended by a factor $f > 1$ only the ones that did not meet the imposed thermalization criterion. In Table 2.1 we report $N_{\text{EMCS}}^{\text{min}}$, the maximum extension factor f_{max} of the simulations, and minimum number N_{τ}^{min} of EMCS in units of τ.

Equilibrium measurements were taken offline over the second half of each simulation. Independently of how much the simulations were extended, we saved $N_{\rm m} = 16$ equally time-spaced configurations and performed measurements on them. We measured four-replica observables. Therefore, for each sample it was possible to choose quadruplets of configurations, each from a different replica, in $N_{\rm m}^4$ ways. Out of the $N_{\rm m}^4$ possibilities, we chose randomly $N_{\rm t} = 1000$ combinations. In other words, each sample participated in the statistics with $N_{\rm t} = 1000$ measurements.

The errors were estimated with the jackknife method (Appendix E).

2.3 Giant Fluctuations and the Silent Majority

2.3.1 No Signs of a Phase Transition with Common Tools

A common way to locate a phase transition is to proceed as described in Sect. 1.3.4, by locating the temperature where the curves $\frac{\xi_L}{L}(T)$ and $R_{12}(T)$ of different lattice sizes cross. For sufficiently large systems, if the curves do not cross, there is no phase transition in the simulated temperature range.

In the present case, this type of analysis yields a clear result: there is no evidence of a crossing at the simulated temperatures, magnetic fields and sizes. This is clearly visible from Fig. 2.1, where the curves $\frac{\xi_L}{L}(T)$ and $R_{12}(T)$ should have some crossing point if we were in the presence of a phase transition. This is in complete qualitative agreement with earlier works on this model [You04, Jör08b].

2.3.2 A Hidden Behavior

Although $\frac{\xi_L}{L}(T)$ is smaller the larger the lattice size, the coherence length ξ_L grows significantly even for our largest lattice sizes. For example at $h = 0.2$, $T = 0.81$ we have $\xi_{16} = 6.09(4)$, $\xi_{24} = 7.63(9)$ and $\xi_{32} = 9.0(2)$. The noticeable size evolution implies that the asymptotic correlation length ξ_∞ is large compared with $L = 32$.

Also, we can examine the behavior of the spin-glass order parameter, the overlap q, by studying its distribution function $P(q)$. In the absence of a phase transition we would be in the paramagnetic phase, and $P(q)$ should be a delta function of a positive overlap $q_{\rm EA}$ (so in finite systems it should be Gaussian).

Instead, we can see from Fig. 2.2 that its distribution $P(q)$ has a very wide support, with tails that, for small enough magnetic fields, reach even negative values of q. This is precisely what was observed in the mean-field version of the model on the de Almeida-Thouless line, and it was attributed to the contribution of few samples [Par12a].

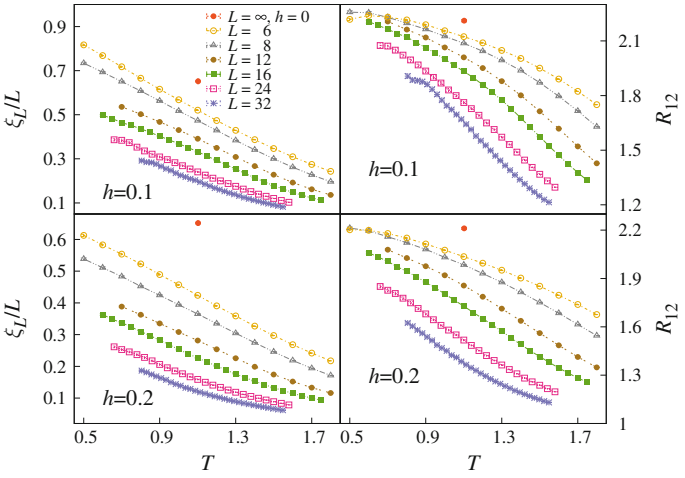

Fig. 2.1 The figures on the *left* show the standard correlation length ξ_L in units of the lattice size L as a function of the temperature T, for all our lattice sizes. The magnetic fields are $h = 0.1$ (*top*), and $h = 0.2$ (*bottom*). If the lattices are large enough, in the presence of a second-order phase transition, the curves are expected to cross at a finite temperature $T_c(h)$. The figures on the *right* show the cumulant R_{12}, which in the presence of a magnetic field is a better indicator of a phase transition [Bn12a], for the same magnetic fields. At zero field the heights of the crossings (which are universal quantities) are indicated with a point at $T_c = 1.1019(29)$. They are $\xi_L/L(h = 0; T_c) = 0.6516(32)$ and $R_{12}(h = 0; T_c) = 2.211(6)$ [BJ13]. In neither case we observe signs of a crossing at the simulated temperatures, nor can we state that the curves will cross at lower temperature. The reader might remark that the curve for $L = 32$, $h = 0.1$ is not as smooth as one would expect from parallel tempering simulations. The reason is twofold. On one side the number of simulated samples is much smaller than for $L < 32$, and on the other side temperature chaos, which is stronger the larger the lattice, is probably present [Fer13]

From these arguments it becomes reasonable to think that we may not be simulating large enough lattices to observe the asymptotic nature of the system and that there may be some hidden behavior that we are not appreciating.

2.3.3 Giant Fluctuations

In fact, we find out that the average values we measure are representative of only a small part of the data set. That is, the average of relevant observables (e.g., the spatial correlation function) only represents the small number of measurements that are dominating it. The rest of the measurements is not appreciated by using the average.

Clearly, standard finite-size scaling methods are not adequate to these systems, and we need to find a way to take into account *all* the measurements. Recalling the wide distributions of Fig. 2.2, it seems reasonable to sort our measurements according

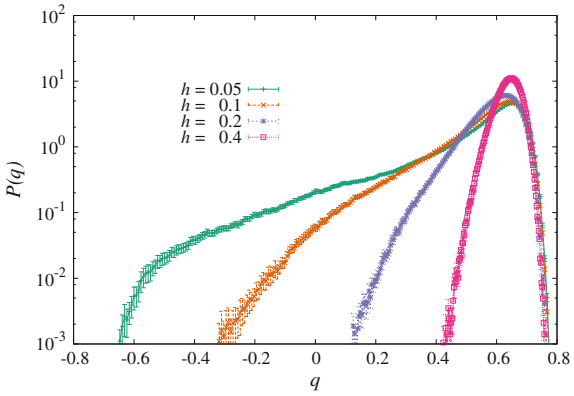

Fig. 2.2 The pdf $P(q)$ of the overlap q, for our largest lattices ($L = 32$) at the lowest simulated temperature ($T = 0.805128$), for all our magnetic fields ($h = 0.05, 0.1, 0.2, 0.4$), see Table 2.1. The order parameter in the EA model is the overlap q, and it is defined in the $[-1, 1]$ interval (see Sect. 1.2.1). The supports are wide, with exponential tails similar to those in the mean-field model at the DAT transition line [Par12a]

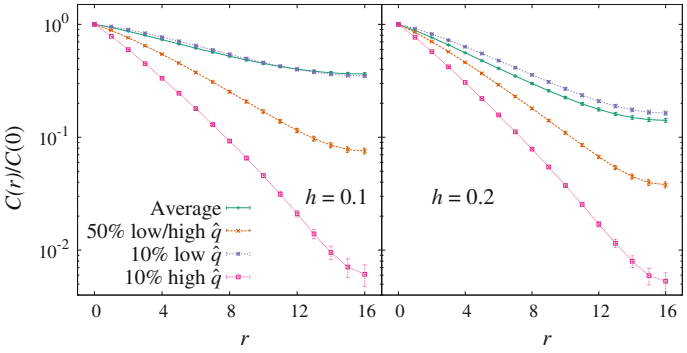

Fig. 2.3 Different instances of the normalised plane correlation function $C(r)$ (Eq. 1.5.3) for $L = 32$, $T = 0.805128$. The field is $h = 0.1$ on the *left*, and $h = 0.2$ in the *right* plot. We sort the measurements with the help of a conditioning variate $\hat{q}$ as described in Sect. 2.4. In this case $\hat{q}$ is the median overlap q_{med}. We show small sets of measurements. Namely, the ones with the 10 % lowest (*top curve*) and highest (*bottom curve*) $\hat{q}$ and those whose $\hat{q}$ corresponds to the median of the distribution of $\hat{q}$ (50 % lowest/highest $\hat{q}$). This sorting reveals extreme differences in the *fauna* of measurements. The average and median of the correlation functions are very different. The average is very similar to the 10 % lowest ranked measures, i.e., it is only representative of a very small part of the data. We normalise $C(r)$ by dividing by $C(0)$ because we measure point-to-plane correlation functions (Eq. 1.5.3). The correlation functions have zero slope at $r = L/2$ due to the periodic boundary conditions

to some conditioning variable $\hat{q}$ related to the overlaps between our replicas (see Sect. 2.4). This way, we find out that the average values we measure are given by only a small part of the measurements. For example in Fig. 2.3 we show the correlation function $C(r)$. We plot 4 estimators of $C(r)$: the average (which is the standard

quantity studied in almost all, if not all, previous work), the $C(r)$ that corresponds to the median of the $\hat{q}$ distribution, and the measurements with the 10 % highest (lowest) value of $\hat{q}$. We see that the average is very close to the 10 % lowest $\hat{q}$, and very far from the two other curves. So, when we plot the average curve, we are only representing the behavior of that small set of data.

Therefore, if we want to understand the behavior of the *whole* collection of measurements, we have to be able to find some criterion to sort them and analyse them separately.

2.4 Conditional Expectation Values and Variances

2.4.1 The Conditioning Variate

As we pointed out in Sect. 2.3, the behavior of the system is dominated by a very small number of measurements.

This means that the average over all the measurements of an observable does not describe the typical behavior of the system. Furthermore, the behavior of the measurements that contribute less to the full averages is qualitatively different from the one of those who give the main contribution (see Fig. 2.3 and later on Sect. 2.9).

We want to classify our measurements in a convenient way, in order to be able to separate different behaviors, and analyse them separately. To this goal, we replace normal expectation values $E(\mathcal{O})$ of a generic observable $\mathcal{O}$, with the expectation value $E(\mathcal{O}|\hat{q})$ conditioned to another random variable $\hat{q}$. Perhaps for lack of imagination $\hat{q}$ will be named CV. For each instance of $\mathcal{O}$ we monitor also the value of $\hat{q}$, and we use it to label $\mathcal{O}$. Hopefully, there will be some correlation.

The conditional expectation value is defined as the average of $\mathcal{O}$, restricted to the measurements i (out of the $\mathcal{N}_{\rm m} = N_{\rm t} N_{\rm samples}$ total measurements) that simultaneously yield $\mathcal{O}_i$ and $\hat{q}_i$ [so we are actually talking about couples of simultaneous measurements $(\mathcal{O}_i, \hat{q}_i)$] in a small interval around $\hat{q} = c$,

$$E(\mathcal{O}|\hat{q} = c) \;=\; \frac{E\left[\mathcal{O}_i \mathcal{X}_{\hat{q}=c}(\hat{q}_i)\right]}{E\left[\mathcal{X}_{\hat{q}=c}(\hat{q}_i)\right]}. \tag{2.2}$$

where we have used the characteristic function

$$\mathcal{X}_c(\hat{q}_i) = \begin{cases} 1, & \text{if } |c - \hat{q}_i| < \epsilon \sim \frac{1}{\sqrt{V}} \\ 0, & \text{otherwise.} \end{cases} \tag{2.3}$$

In Appendix C we give technical details on the choice of ϵ. To make notation lighter, in the rest of the paper we will replace $E(\mathcal{O}|\hat{q} = c)$ with $E(\mathcal{O}|\hat{q})$.

The traditional expectation value $E(\mathcal{O})$ can be recovered by integrating over all the possible values of the CV $\hat{q}$:

$$E(\mathcal{O}) = \int d\hat{q}\; E(\mathcal{O}|\hat{q})P(\hat{q}), \quad P(\hat{q}) = E[\mathcal{X}_{\hat{q}}], \tag{2.4}$$

where $P(\hat{q})$ is the probability distribution function of the CV.

We remark that the concept of CV is fairly similar to the one of control-variate. Yet, the latter was formalised slightly differently, and with the objective of enhancing the precision of the measures [Fer09a]. In [AB10a, AB10b] a procedure very similar to the present one was followed, but the aim was constructing clustering correlation functions, while in our case the CV is used to analyse *separately* different behaviors outcoming from the same global data set, so that a sensible finite-size scaling becomes possible.

2.4.2 Measurements Against Samples

The reader may argue that a sample-to-sample distinction of the different behaviors is more natural than a measurement-dependent one (although intuition leads to assume that the two are related). This was indeed our first approach to the problem (it was, in fact, proposed in [Par12a]). However, we found that the approach described in the previous section is preferable, both for practical and conceptual reasons.

On the practical side, a sample-to-sample separation implies that from each sample we get only one data point: For any observable, we limit ourselves to its thermal average. In this case we would need a limitless amount of samples to be able to construct a reasonable $P(\hat{q})$. Moreover, the simulations should last a huge number of autocorrelation times τ if we want to have small enough errors on the thermal averages of each sample. Otherwise, we would introduce a large bias that is not reduced when increasing the number of samples.

On the conceptual side, representing each sample merely with a single number (namely the thermal expectation value), is a severe oversimplification. As we show in Fig. 2.4, even though we are in the paramagnetic phase, the behavior within each sample is far from trivial. For a non-negligible fraction of the samples, the overlap distribution is wide, often with a multi-peak structure. The barriers among peaks can be deep, hence suggesting extremely slow dynamics (which is indeed the case for physical dinamics [BJ14b], or for the parallel tempering dynamics [Huk96, Mar98]).

In summary, we find that using instantaneous measurements to classify the available information is the best solution.

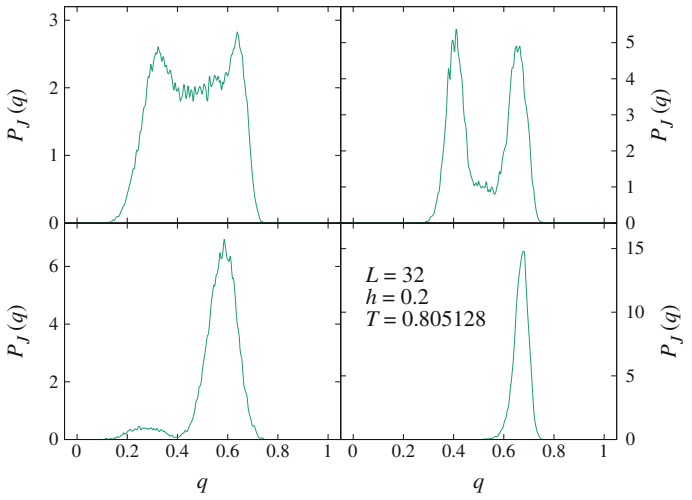

Fig. 2.4 Sample-dependent pdfs $P_J(q)$, for four different samples, each representing a different type of $P_J(q)$ we encountered. As well as the averaged $P(q)$, also the sample-dependent density function can be wide and with a structure. The plotted data comes from samples with $L = 32$, $h = 0.2$ and $T = 0.805128$

2.4.3 The Selection of the Conditioning Variate

2.4.3.1 A Quantitative Criterion

In Appendix D we show how to decompose the moments of a generic variable $\mathcal{O}$ as sums of averages conditioned to $\hat{q}$. For the variance we find that

$$\mathrm{var}(\mathcal{O}) = \int_{-1}^{1} d\hat{q}\; P(\hat{q}) \left\{ \mathrm{var}(\mathcal{O}|\hat{q}) + \left[E(\mathcal{O}) - E(\mathcal{O}|\hat{q}) \right]^2 \right\}, \tag{2.5}$$

where

$$\mathrm{var}(\mathcal{O}|\hat{q}) = E\left(\left[\mathcal{O} - E(\mathcal{O}|\hat{q}) \right]^2 \mid \hat{q} \right). \tag{2.6}$$

A convenient CV is the one that mostly discerns the different behaviors of the model. We can get a quantitative criterion for the selection of a good $\hat{q}$ by rewriting Eq. (2.5) as:

$$\mathrm{var}(\mathcal{O}) = c_1 + c_2, \tag{2.7}$$

where

$$c_1 \equiv \int_{-1}^{1} d\hat{q}\; P(\hat{q}) \mathrm{var}(\mathcal{O}|\hat{q}),$$

$$c_2 \equiv \int_{-1}^{1} d\hat{q}\; P(\hat{q})[E(\mathcal{O}) - E(\mathcal{O}|\hat{q})]^2, \tag{2.8}$$

and studying the relation between the terms c_1 and c_2. Both are positive, and their sum is fixed independently from the used CV.

We will show intuitively that a useful CV has $c_2 \gg c_1$.

If $c_1 = 0$ the fluctuations of $\mathcal{O}$ would be explained solely by the fluctuations of $\hat{q}$. In this case c_2 is large and assumes its largest possible value, meaning that different values of $\mathcal{O}$ are mostly spread apart by $\hat{q}$.

On the other side, $c_2 = 0$ implies $E(\mathcal{O}) = E(\mathcal{O}|\hat{q})$ and signals an insensitive CV, with null correlation between $\mathcal{O}$ and $\hat{q}$.

Equations (2.7) and (2.8) can thus be used to quantify the quality of the CV $\hat{q}$: We look for the highest quotient c_2/c_1.

2.4.3.2 Candidates for $\hat{q}$

To select an appropriate CV we need to chose $\mathcal{O}$ and propose some test definitions for $\hat{q}$. The functions of the observables that one could use as a CV are infinite, but physical intuition lead us to try with simple functions of the overlap and of the link overlap Eq. (1.21). On the other side, a natural choice of $\mathcal{O}$ is the estimator of the replicon susceptibility [see Eq. (1.64)]. This means that

$$\mathcal{O} \longrightarrow \frac{1}{3\mathcal{N}} \sum_{\substack{\text{equiv.wave} \\ \text{vectors } \boldsymbol{k}}}^{\mathcal{N}} \left[|\Phi_{\boldsymbol{k}}^{(ab;cd)}|^2 + |\Phi_{\boldsymbol{k}}^{(ac;bd)}|^2 + |\Phi_{\boldsymbol{k}}^{(ad;bc)}|^2 \right], \tag{2.9}$$

where $\mathcal{N}$ is the number of equivalent wave vectors one can construct. This is a 4-replica quantity [see Appendix (B.9)], so six instantaneous overlaps (and six link overlaps) are associated to each instance of the correlators. To define $\hat{q}$ we need to propose a function of the six overlaps in order to get a one-to-one correspondence.

Let us reorder each 6-plet of instantaneous overlaps $\{q^{(ij)}\}$ in the form of six sorted overlaps $\{q_k\}$

$$\left\{q^{(ab)}, q^{(ac)}, q^{(ad)}, q^{(bc)}, q^{(bd)}, q^{(cd)}\right\} \longrightarrow \{q_1 \le q_2 \le q_3 \le q_4 \le q_5 \le q_6\}, \tag{2.10}$$

and do the same thing with the link overlap

$$\begin{aligned} &\left\{q_{\text{link}}^{(ab)},\ q_{\text{link}}^{(ac)},\ q_{\text{link}}^{(ad)},\ q_{\text{link}}^{(bc)},\ q_{\text{link}}^{(bd)},\ q_{\text{link}}^{(cd)}\right\} \longrightarrow \\ &\longrightarrow \left\{q_{\text{link},1} \le q_{\text{link},2} \le q_{\text{link},3} \le q_{\text{link},4} \le q_{\text{link},5} \le q_{\text{link},6}\right\}, \end{aligned} \tag{2.11}$$

Table 2.2 Criterion for the choice of the CV $\hat{q}$ for $h = 0.1$, $L = 32$, $T = 0.805128$, by looking at the indicators c_1 and c_2 relatively to $\chi_{\mathrm{R}}(\mathbf{0})$ and $\chi_{\mathrm{R}}^{\mathrm{link}}(\mathbf{0})$

$\hat{q}$	$\chi_R^{\mathrm{spin}}: c_1$	$\chi_R^{\mathrm{spin}}: c_2$	c_2/c_1	$\chi_R^{\mathrm{link}}: c_1$	$\chi_R^{\mathrm{link}}: c_2$	c_2/c_1
$q_{\mathrm{min}}^{\mathrm{spin}}$	399000 ± 37000	121000 ± 15000	0.30(6)	8.35 ± 0.47	0.297 ± 0.023	0.36(5)
$q_{\mathrm{max}}^{\mathrm{spin}}$	514000 ± 51000	6230 ± 690	0.012(3)	8.54 ± 0.49	0.1070± 0.0073	0.013(2)
$q_{\mathrm{med}}^{\mathrm{spin}}$	162000 ± 10000	358000 ± 45000	2.2(4)	7.35 ± 0.39	1.30 ± 0.11	0.18(2)
$q_{\mathrm{av}}^{\mathrm{spin}}$	328000 ± 26000	192000 ± 28000	0.6(1)	7.51 ± 0.41	1.141 ± 0.094	0.15(2)
$q_{\mathrm{min}}^{\mathrm{link}}$	461000 ± 46000	59300 ± 5800	0.13(3)	8.38 ± 0.48	0.271 ± 0.020	0.032(4)
$q_{\mathrm{max}}^{\mathrm{link}}$	460000 ± 46000	59700 ± 5900	0.13(3)	8.56 ± 0.49	0.0838± 0.0067	0.010(1)
$q_{\mathrm{med}}^{\mathrm{link}}$	360000 ± 36000	160000 ± 18000	0.44(9)	7.36 ± 0.38	1.29 ± 0.11	0.17(2)
$q_{\mathrm{av}}^{\mathrm{link}}$	415000 ± 42000	105000 ± 10000	.25(5)	7.72 ± 0.42	0.927 ± 0.073	0.12(2)

We want the $\hat{q}$ to split as much as possible the different measured susceptibilities. This is obtained, see (2.8), when the ratio c_2/c_1 is maximised. From the data we see that this occurs with $\hat{q} = q_{\mathrm{med}}$

The following are natural test CVs:

$$\hat{q} = \begin{cases} q_{\mathrm{min}} &= q_1 & \text{(the minimum)} \\ q_{\mathrm{link,min}} &= q_{\mathrm{link},1} & \\ q_{\mathrm{max}} &= q_6 & \text{(the maximum)} \\ q_{\mathrm{link,max}} &= q_{\mathrm{link},6} & \\ q_{\mathrm{med}} &= \frac{1}{2}(q_3 + q_4) & \text{(the median)} \\ q_{\mathrm{link,med}} &= \frac{1}{2}(q_{\mathrm{link},3} + q_{\mathrm{link},4}) & \\ q_{\mathrm{av}} &= \frac{1}{6}(q_1 + q_2 + q_3 + q_4 + q_5 + q_6) & \text{(the average)} \\ q_{\mathrm{link,av}} &= \frac{1}{6}(q_{\mathrm{link},1} + q_{\mathrm{link},2} + q_{\mathrm{link},3} + q_{\mathrm{link},4} + q_{\mathrm{link},5} + q_{\mathrm{link},6}). & \end{cases} \tag{2.12}$$

We checked how each of the CVs sorted the overlap and link susceptibilities $\chi_{\mathrm{R}}(\mathbf{0})$ and $\chi_{\mathrm{R}}^{\mathrm{link}}(\mathbf{0})$. Table 2.2 depicts the c_1 and c_2 terms, and their ratio, for all the CV, for a single triplet (T, L, h) and $\boldsymbol{k} = (0, 0, 0)$.

The best CV is clearly the median overlap, since it has the highest c_2/c_1 ratio. The situation is similar for other choices of (T, L, h).

For a qualitative description of the difference between the diverse CVs, in Fig. 2.5 (top) the reader can appreciate the probability distribution functions for each of the CVs, while in Fig. 2.5 (bottom) we plotted the conditioned susceptibilities. From (2.4) we stress that the integral of the values on the top times the values of the bottom set yields the average susceptibility, which is indicated with a horizontal line on the

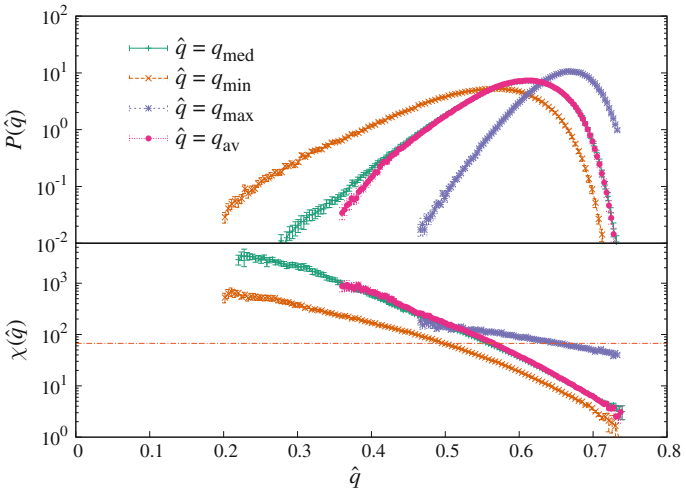

Fig. 2.5 Features of the diverse CVs we proposed for $L = 32$, $h = 0.2$ and $T = 0.805128$. The *top* figure shows the histograms $P(\hat{q})$ for four candidates of conditioning variate: the minimum overlap $q_{\rm min}$ [of the six we can make with four replicas, recall equations (2.12)], the maximum $q_{\rm max}$, the median $q_{\rm med}$ and the average $q_{\rm av}$. The histograms were constructed as explained in Appendix C. The *bottom* figure depicts the size of the susceptibility χ for each value of the CV. The horizontal line marks the value of χ when it is averaged over the full set of measurements. For aesthetic reasons in both figures we have cut the curves at the two end points, where they become extremely noisy due to poor sampling

bottom plot of Fig. 2.5. As it is also reflected by Table 2.2, $q_{\rm max}$ is the worst CV, as its χ does not vary much with the fluctuations of $q_{\rm max}$. The steepest slope is obtained when the CV is $q_{\rm av}$ or $q_{\rm med}$, but the latter is smoother and covers a wider range of χ.

Figure 2.5 also displays the large deviations present in the system. In fact one can see that the value of $q_{\rm med}$ at which the $P(q_{\rm med})$ has its maximum is significantly different with respect to the value of $q_{\rm med}$ at which $\chi(q_{\rm med})$ assumes the value of the average.

Let us compare the overlap with the link-overlap signal. Besides the fact that the link overlaps appear to be bad CVs, one can see from Table 2.2 that on one side the fluctuations on $\chi_{\rm link,R}(\mathbf{0})$ are much smaller than $\chi_{\rm R}(\mathbf{0})$, and on the other none of the CVs seems to separate the behaviors (the ratio c_2/c_1 is much smaller). We can see this better from Fig. 2.6, that depicts the results of a sorting with the median (link-)overlap on $C_{\rm R}(\boldsymbol{r})$ and $C_{\rm link,R}(\boldsymbol{r})$. The bold line stands for the average behavior, while the thin ones represent a sorting of the data according to the quantile of the distribution of the CV.[5] If the average is in the middle of the thin lines it is a good descriptor of the data, otherwise it is a biased estimator. Very spread thin lines indicate that $c_2 \gg c_1$: the CV separates behaviors properly.

[5] A quantile is the value of $\hat{q}$ that separates a fixed part of the pdf (Sect. 2.5 later on).

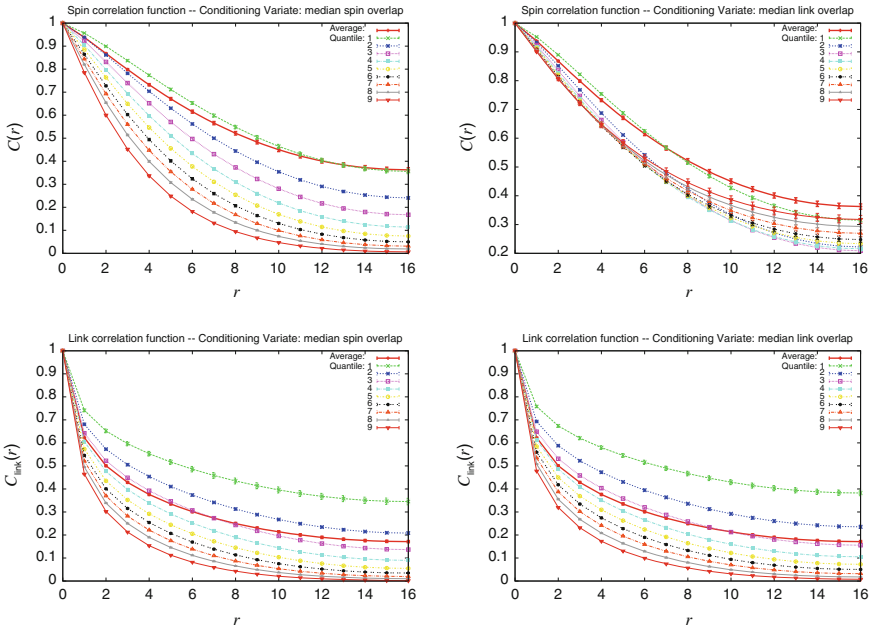

Fig. 2.6 Spin and link plane replicon correlation functions with $h = 0.1$, $L = 32$, $T = 0.805128$. The thin lines indicate different quantiles of the conditioning variate's distribution (see Sect. 2.5), the bold lines indicate the average. *Top* Spin correlation functions, *bottom* link correlation functions. *Left* $\hat{q} = q_{\text{med}}$, *right*: $\hat{q} = q_{\text{link,med}}$. Discussion in the main text

The data illustrates that, while the average spin correlation function is not representative of the majority of outcomes for both the CV, the link correlation function is well-described by its average. This suggests that the link overlap might be a more accurate indicator of the critical behavior of the EA spin glass in a field. Analyses on the link-overlaps will be object of further future studies.

On another side, if we concentrate on the spin correlation function $C(r)$, we see that the link is not a suitable CV, both because it separates less the behaviors, and because the separation has a dependency on the distance r.

2.5 Quantiles and a Modified Finite-Size Scaling Ansatz

We stated in Sect. 2.3 that the set of measurements with low $\hat{q}$ has a very different behavior from the measurements with high $\hat{q}$ (recall Fig. 2.3). From now on, we shall restrict ourselves to $\hat{q} = q_{\text{med}}$, since we evinced that the median is our best CV. Our next goal will be to carry out a finite-size scaling analysis based on the $P(q_{\text{med}})$ that lets us observe different parts of the spectrum of behaviors of the system.

In order to analyse separately these different sets of measures, we divide the $P(q_{\text{med}})$ in 10 sectors, each containing 10 % of the measured q_{med}. We focus our analysis on the values of q_{med} that separate each of these sectors. They are called quantiles (see, e.g., [Hyn96]), and we label them with the subscript $i = 1, \ldots, 9$. If we call $\tilde{q}_i(h, T, L)$ the value of the i^{th} quantile, we can define it in the following implicit way:

$$\int_{-1}^{\tilde{q}_i} \mathrm{d}\hat{q}\, P(\hat{q}) = \frac{i}{10}. \tag{2.13}$$

In Appendix C we explain how $\tilde{q}_i(h, T, L)$ was computed.

We can adapt to the ith quantile the definitions we gave in Sect. 1.2.4:

$$\chi_{\text{R},i}(\boldsymbol{k}) = \frac{1}{N} E\left(|\hat{\Phi}_{\boldsymbol{k}}^{(ab;cd)}|^2 \,\middle|\, \tilde{q}_i \right), \tag{2.14}$$

$$\xi_{L,i} = \frac{1}{2\sin(k_{\min}/2)} \sqrt{\frac{\chi_{\text{R},i}(\boldsymbol{0})}{\chi_{\text{R},i}(2\pi/L, 0, 0)} - 1}, \tag{2.15}$$

$$R_{12,i} = \frac{\chi_{\text{R},i}(2\pi/L, 0, 0)}{\chi_{\text{R},i}(2\pi/L, \pm 2\pi/L, 0)}. \tag{2.16}$$

This way we can extend the finite-size scaling methodology to the ith quantile:

$$\left.\frac{\xi_L}{L}\right|_{T,h,L,i} = f_{\xi_i}\left(L^{1/\nu}(T - T_{\text{c}})\right) + \cdots, \tag{2.17}$$

$$R_{12}|_{T,h,L,i} = f_{R_i}\left(L^{1/\nu}(T - T_{\text{c}})\right) + \cdots. \tag{2.18}$$

This is a new approach for finite-size scaling. Although it demands a very large amount of data because it is done over a small fraction of the measurements (in Appendix E we explain a method we used to reduce rounding errors), it allows us to perform finite-size scaling on selected sets of measurements.

Let us stress that no a priori knowledge is required on the probability distribution function $P(q_{\text{med}})$: Quantiles are conceived in order to define a scaling that self-adapts when the volume increases.

2.6 Testing the Quantile Approach

We take advantage of our $h = 0$ data from [BJ13] to validate our new FSS ansatz and the quantile description, by showing its behavior in the zero-field case. Two replicas would be enough to construct connected correlators in $h = 0$, and using the 4-replica definitions proposed in Sect. 1.2.4 only adds noise to the results. Yet, we opted for the latter option because the objective of the current section is the validation of the full procedure proposed herein.

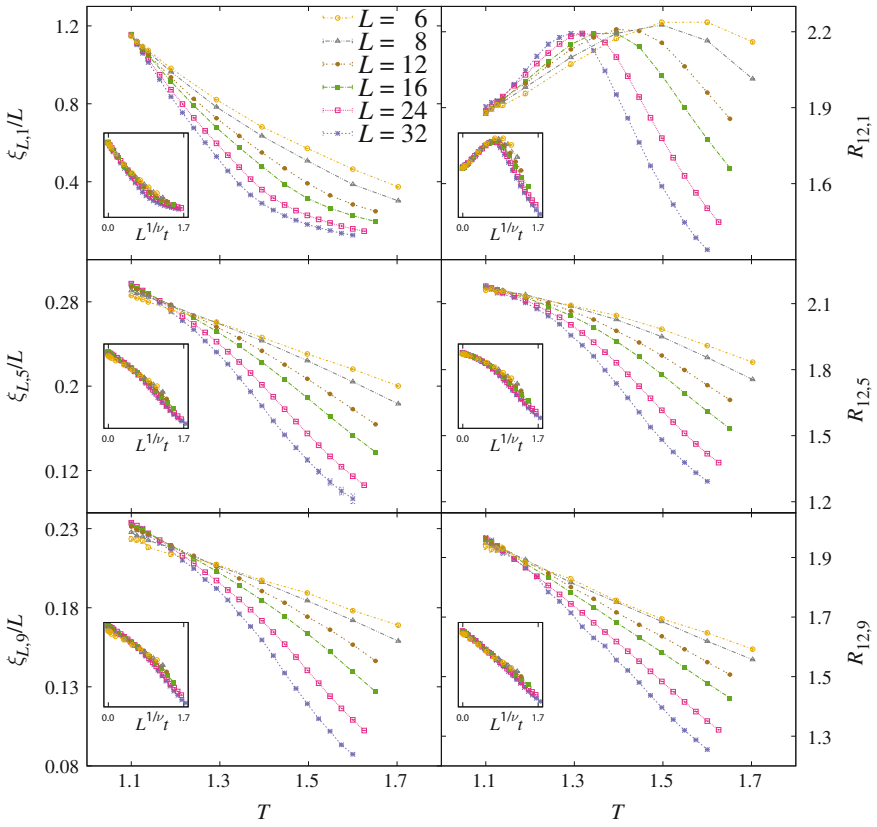

Fig. 2.7 Finite-size indicators of a phase transition, computed for $h = 0.2$. On the *left* side we plot, for quantiles 1 (*top*), 5 (*middle*) and 9 (*bottom*), the correlation length in units of the lattice size ξ_L/L versus the temperature, for all our lattice sizes. The *right* side is equivalent, but for the R_{12}, defined in Eq. (1.46). The curves crossings are compatible with the well-known temperature of the zero-field transition. The data come from [BJ13]. We used 256,000 samples for each lattice size. The *insets* show the same data of the larger sets, but as a function of the scaling variable $L^{1/\nu}t$, where t is the reduced temperature $t = (T - T_c)/T_c$

In the absence of a magnetic field we expect that the curves $\xi/L(T)$ and R_{12} cross no matter the quantile, since the behavior of the system is not dominated by extreme events and crossover fluctuations. Also, in this case the data in our hands arrive down to the critical point, so the crossings ought to be visible.

One can see in fact from Fig. 2.7 that all the quantiles show visible signs of a crossing at T_c both in the case of ξ_L/L and of R_{12}. Furthermore, if we plot the same data as a function of the scaling variable $L^{1/\nu}(T - T_c)/T_c$ the data collapses well for all the quantiles (Fig. 2.7, insets).

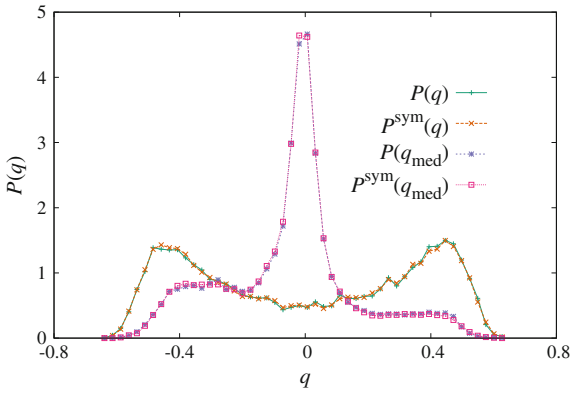

Fig. 2.8 Probability distribution function for $h = 0$, $L = 24$, $T = 1.1$. The data come from 512 samples where we took all the 16^4 combinations of overlaps per sample. We show $P(q)$, that in null field is symmetric, and $P(q_{\rm med})$, that is not. We also plot the symmetrized histograms $P^{(\rm sym)}(q)$ and $P^{(\rm sym)}(q_{\rm med})$, that overlap on the respective curves. As more extendedly explained in the main text, the symmetrized overlap is obtained by averaging each $q_{\rm med}$ over the values it would acquire by imposing all the combinations of Z_2 symmetry (flip all the spins) on the configurations on which the $q_{\rm med}$ is calculated

Some reader may be surprised that quantiles 1 and 9 show different behavior, being $P(q)$ symmetrical (Fig. 2.8). The reason is that, although $P(q)$ is symmetrical, $P(q_{\rm med})$ is not. In fact, given six overlaps $q^{\rm ab}$, $q^{\rm ac}$, $q^{\rm ad}$, $q^{\rm bc}$, $q^{\rm bd}$, $q^{\rm cd}$ coming from four configurations $|s^{(\rm a)}\rangle$,$|s^{(\rm b)}\rangle$,$|s^{(\rm c)}\rangle$,$|s^{(\rm d)}\rangle$, each enjoying a Z_2 symmetry, the distribution of their median privileges negative values.[6] We show this in Fig. 2.8, where we give both the $P(q)$ and the $P(q_{\rm med})$ for $h = 0$, $L = 32$, $T = 1.1$. The first is symmetrical and the second is not. To convince the reader that the starting configurations do enjoy Z_2 symmetry, we also construct the symmetrized functions $P^{(\rm sym)}(q)$ and $P^{(\rm sym)}(q_{\rm med})$. These two functions are obtained by explicitly imposing the reflection symmetry Z_2: for each measurement we construct the 2^4 overlaps with both $|s\rangle$ and $|-s\rangle$. It is visible from Fig. 2.8 that $P^{(\rm sym)}(q_{\rm med})$ is asymmetric even though we imposed by hand the Z_2 symmetry on the configurations.

[6] Let us give a simple example. Take 4 Z_2-symmetric single-spin systems that can assume different values $s_1 = \pm 1$, $s_2 = \pm 2$, $s_3 = \pm 3$, $s_4 = \pm 4$. We can construct 6 overlaps $q_{ij}(s_1, s_2, s_3, s_4)$. If we explicitate the Z_2 symmetry, taking all the combinations of our random variables, the histogram of q will be symmetric with zero mean. Yet, if we take the histogram of the median overlap, it will be asymmetric with mean $\langle q_{\rm med}\rangle = -3$. This can easily be checked by computing all the possible combinations of the signs of the s_i and computing the median in each case: $q_{\rm med}(+1, +2, +3, +4) = 5$, $q_{\rm med}(+1, +2, +3, -4) = -1$, $q_{\rm med}(+1, +2, -3, -4) = -3.5$, and so on.

2.6.1 The $P(q_{\mathrm{med}})$

To our knowledge, the median overlap q_{med}, despite its simplicity, has not been object of previous study. Yet, since we base our analysis on this quantity, it is necessary to dedicate passing attention to its features.

By its definition, the probability distribution $P(q_{\mathrm{med}})$ of the median overlap has narrower tails than $P(q)$ (recall Fig. 2.2), although from Fig. 2.5 (top) it is clear that the strong fluctuations persist also with q_{med}.

The median of $P(q_{\mathrm{med}})$ corresponds to the fifth quantile. We will prefer to call it "5th quantile" rather than "median of the median overlap". Of the nine studied quantiles it is the smoothest and has the least finite-size effects, as one can see from Fig. 2.9 (inset). Further analysis is given in Sect. 2.8.

We remark also that the separation between the different $\tilde{q}_i$'s can be used as order parameter, since its thermodynamic limit should be zero in the paramagnetic phase, and greater than zero in the possible low-temperature phase due to the (would-be) replica symmetry breaking. Figure 2.9 shows the difference between the 8th and the 2nd quantile, i.e., the q_{med}-span of the central 60 % of the data. If we were able to extrapolate a clean $L \to \infty$ limit for this curve, we would be able to answer to whether the transition exists or not. Unfortunately, even for $T > T_c(h = 0) = 1.1019(29)$, where we know that we are in the paramagnetic phase, it is not possible to make good extrapolations since the trend is strongly non-linear. In Sect. 2.8 we will show that extrapolations to the thermodynamic limit were only possible in the trivial case of

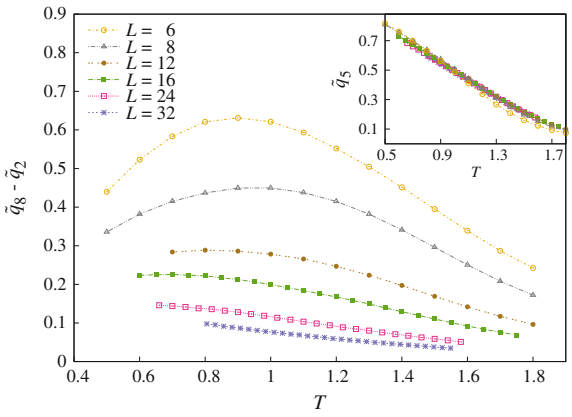

Fig. 2.9 Using q_{med} as CV, we show the temperature dependence of the difference between quantiles $\tilde{q}_8 - \tilde{q}_2$, for all our lattice sizes, in a field of intensity $h = 0.2$. This corresponds to the width of the central 60 % of area of $P(q_{\mathrm{med}})$. This quantity can reveal a phase transition, since in the paramagnetic phase the $P(q_{\mathrm{med}})$ should be a delta function, while in the spin-glass phase it should have a finite support. We show the central 60 % and not a wider range because it is an equivalent indicator of the phase transition, and it is safer from rare events that would vanish in the thermodynamic limit. In the *inset* we show the position of 5th quantile as a function of temperature in all our lattice sizes. It is a very smooth curve with very small finite-size effects

$h = 0.4$ (deep paramagnetic phase), and that between all the quantiles, the median curve is the one that shows less finite-size effects.

2.7 A *caveat* for the Quantile Description

In the absence of an applied field, the overlap probability distribution function $P(q)$ is symmetric, with a single peak centred in $q = 0$. In the presence of a field, instead, we expect the $P(q)$ to be strictly positive, at least in the thermodynamic limit. Similarly, we expect that the probability distribution function $P(q_{\text{med}})$ have only one peak at positive q_{med} when a field is applied, and a peak in $q = 0$ if $h = 0$.

If the system sizes are too small, it may occur that the $h = 0$ behavior bias the $P(q_{\text{med}})$. This is what happens, for example, when $L = 6$, $h = 0.2$ and the temperature is sufficiently low: a second peak around $q_{\text{med}} \simeq 0$ develops upon lowering T (Fig. 2.10, top). This second peak disappears when we increase the lattice size (Fig. 2.10, centre), and the $P(q_{\text{med}})$ assumes only positive values when L is large enough (Fig. 2.10, bottom). The lower the field, the easier it is to find multiple peaks, and the greater the system has to be to be able to neglect the $h = 0$ behavior. For $h = 0.05$, even lattices with $L = 12$ show a double peak.

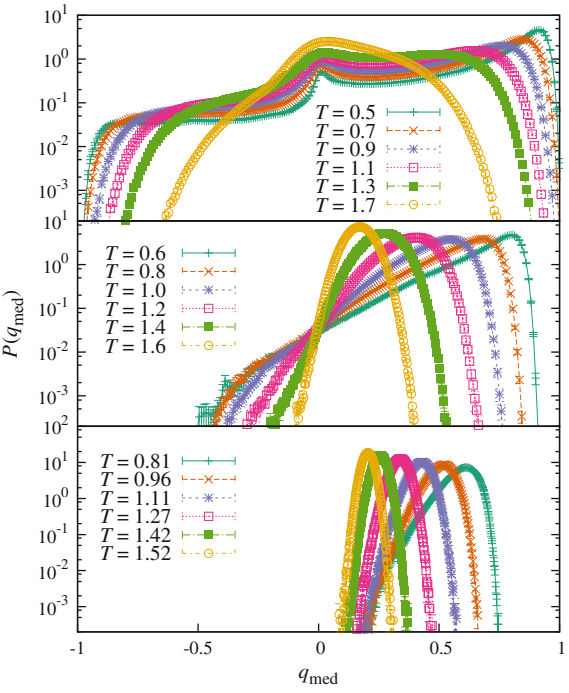

Fig. 2.10 Median overlap probability distribution function $P(q_{\text{med}})$ with $h = 0.2$ for different temperatures (the ones from $L = 32$ are an approximation to the second decimal digit). The *top* figure shows the case of $L = 6$, where the lowest temperature curves display a second peak around $q_{\text{med}} \simeq 0$, which disappears when T increases. For $L = 16$ (*middle*) the $P(q_{\text{med}})$ are single-peaked, but assume also negative values. In the *bottom* curve we have $L = 32$, where the $P(q_{\text{med}})$ are single-peaked and defined only on positive q_{med}, since we are closest to the asymptotic behavior

A second peak in $P(q_{\rm med})$ is a clear signal that we are observing and echo of $h = 0$. When we make the quantile classification, and have a quantile on a peak, we are seeing *only* non-asymptotic data. Thus, quantile 1 for the smallest lattices gives us no relevant information.

If we plot versus the temperature any observable $\mathcal{O}$ related to the first quantile, the information will be biased for low temperatures, and the bias will gradually disappear as we increase T. The result is that the curve $\mathcal{O}(T)$ will have a strange shape and will be of no use (see, e.g., the $h = 0.05$ data in Fig. 2.11). This is why we did not include the $L = 6$ points in the top set of Fig. 2.13 later on.

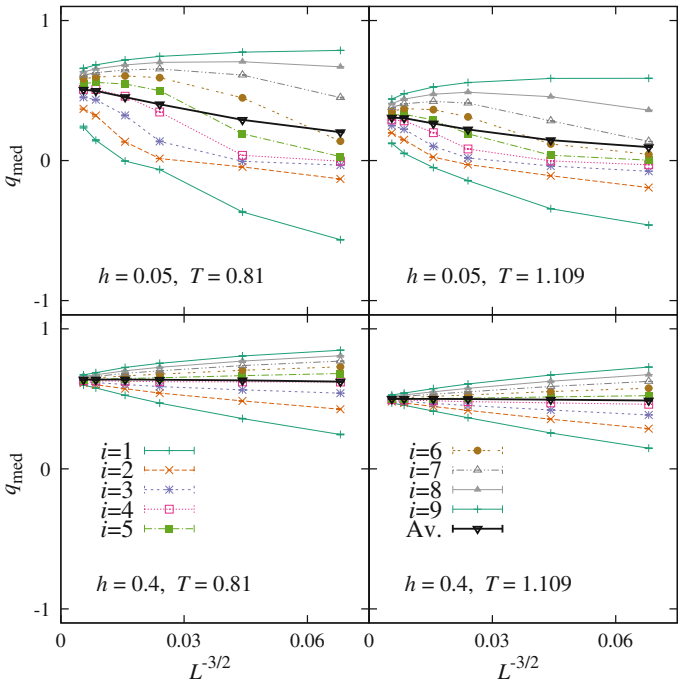

Fig. 2.11 Extrapolations to infinite size of the quantile overlap $\tilde{q}_i$, for $T = 0.81$ (*left*) and $T = 1.109$ (*right*), and fields $h = 0.05$ (*top*) and $h = 0.4$ (*bottom*). We show quantiles $i = 1, \ldots, 9$ (*thin lines*), and the average behavior (*bold line*). The $h = 0.4$ extrapolations to infinite volume were clean ($\chi^2/\mathrm{DOF} < 1$), while for $h = 0.05$ (and all the other fields we simulated), we encountered too strong and nonlinear finite-size effects to get reasonable extrapolations. We choose $1/L^{D/2}$ as scaling variable because in conditions of validity of the central limit theorem, the fluctuations should be of order $1/\sqrt{N}$

2.8 Finding a Privileged q

Since all our simulations are in the paramagnetic phase the thermodynamic limit of the $P(q)$ is a delta function, so all the quantiles should tend to the a common $q = q_{\mathrm{EA}}$ in the $L \to \infty$ limit. We tried to perform these extrapolations at fixed (reasonably low) temperature, to see if we could look at the problem from such a privileged position. In Fig. 2.11 we see this type of extrapolation for $h = 0.4$ and $h = 0.05$, at temperatures $T = 0.81$ and 1.109. The first is the lowest temperature we simulated in all our lattices, while the second is the zero-field critical temperature [BJ13]. Since we are in the paramagnetic phase and we are plotting $\tilde{q}_i$ versus the inverse lattice size, the curves should cross at the intercept. This is indeed what appears to happen, but although in the case of $h = 0.4$, the extrapolations were clean, for all the other simulated fields the finite-size effects were too strong and nonlinear to make solid extrapolations. We remark, yet, that once $L > 8$ the 5th quantile is the one with the least finite-size effects.

2.9 The Silent Majority

As already emphasized, the behavior of the system is characterized by very strong fluctuations, and a wide and asymmetric $P(q)$. As a result, the average and median behavior are very different. In Fig. 2.12, we show the replicon susceptibility: its average χ on the left plot, and its fifth quantile χ_5. Motivated by the arguments in Sect. 2.4 all the quantiles we show in this section use the CV $\hat{q} = q_{\mathrm{med}}$.

Visibly, not only is the average susceptibility much larger than the 5th quantile, but also the two have peaks at different temperatures. Also, finite-size effects are much stronger in the case of χ_5 (yet, recall the inset in Fig. 2.9, finite-size effects on $\tilde{q}_5$ are tiny).[7]

We show in Fig. 2.13 how sorting the data with the quantiles revealed the presence of different types of behavior, by plotting the ξ_L/L and the R_{12} for quantiles 1, 5 and 9 at $h = 0.2$. There are two vertical lines in each figure. The one on the left represents the upper bound $T^{\mathrm{up}}(h)$ for the phase transition (meaning that no phase transition can occur for $T > T^{\mathrm{up}}(h)$) given in [BJ14b], while the one on the right indicates the zero field critical temperature $T_{\mathrm{c}} = 1.1019(29)$ [BJ13].

We can see that the 1st quantile has the same qualitative behavior of the average (Fig. 2.1), but lower values, since the main contribution to the average comes from data whose q_{med} is even lower than $\tilde{q}_1$. Moreover, one can notice that in Fig. 2.1 the indicators ξ_L/L and R_{12} show a different qualitative behavior when the lattices are small (R_{12} shows a crossing). This discrepancy vanishes when we look only at the

[7] We made power law extrapolations to $L \to \infty$ of the maxima of the susceptibility, but they were not satisfactory (too large χ^2/DOF). Only for $h = 0.2, 0.4$ were we able to fit the maxima's heights and obtained $\eta(h = 0.2) \approx 0.6$ and $\eta(h = 0.4) \approx 0.9$..

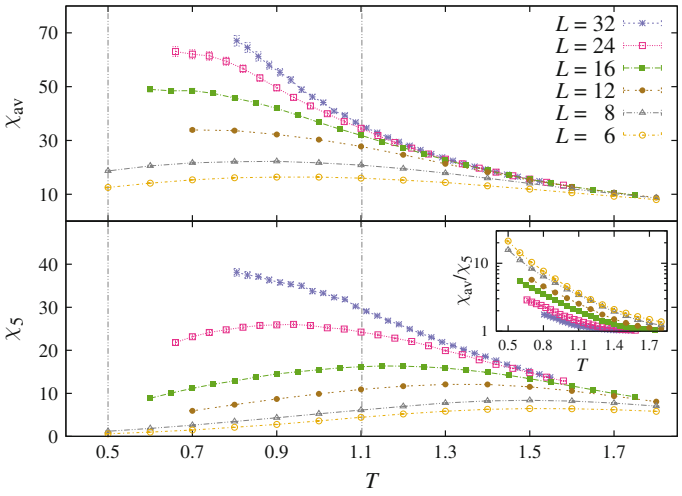

Fig. 2.12 The replicon susceptibility χ as a function of the temperature, for all the simulated lattice sizes and the field $h = 0.2$. We represent its average χ (*top*), and the 5th quantile χ_5 with $\hat{q} = q_{\text{med}}$ (*bottom*). In both plots, the two vertical lines represent the upper bound of the possible phase transition $T^{\text{up}}(h = 0.2) = 0.5$ given in [BJ14b], and the zero-field critical temperature $T_c(h = 0) = 1.109(29)$ [BJ13]. The amplitudes and the positions of the peaks of χ are strikingly different (mind the different scales in the y axes). The *inset* shows the ratio between the two, which we expect to tend to an order one constant in the thermodynamic limit. This is actually what we see at high temperatures

first quantile: Separating different behaviors enhances the consistency between ξ_L/L and R_{12}.

The behavior of the 5th quantile is quite different, since now it appears reasonable that the curves cross at some $T \lesssim T^{\text{up}}(h)$. The crossings become even more evident when we consider the highest quantile.

All this is consistent with the arguments of Sect. 2.3, where we showed how the correlation function is dominated by a little portion of data, near the first quantile (Fig. 2.3), while the behavior of the majority of the samples is hidden.

Unfortunately, the high non-linearity of the curves impedes an extrapolation of the crossing points, but they are apparently compatible with the upper bound T^{up}, and their heights apparently do not depend on the intensity of the applied field h (see also Fig. 2.14).

The careful reader might have noticed that the upper bound $T^{\text{up}}(h)$ for the possible phase transition given in [BJ14b] is higher when the field is lower: $T^{\text{up}}(0.1) = 0.8 > T^{\text{up}}(0.2) = 0.5$. It is then justified to ask oneself how do the quantile plots look like for $h = 0.1$. We show them in Fig. 2.14. Since the field is lower, the effects on the double peak on the first quantile (Sect. 2.7) extend to larger lattices than for $h = 0.2$. Thus, we show only the non-biased sizes, i.e., $L > 12$.

Although the 9th quantile shows signs of scale invariance at $T = T^{\text{up}}(0.1)$, the behavior of the 5th quantile suggests a scale invariance around $T = 0.5$. We believe

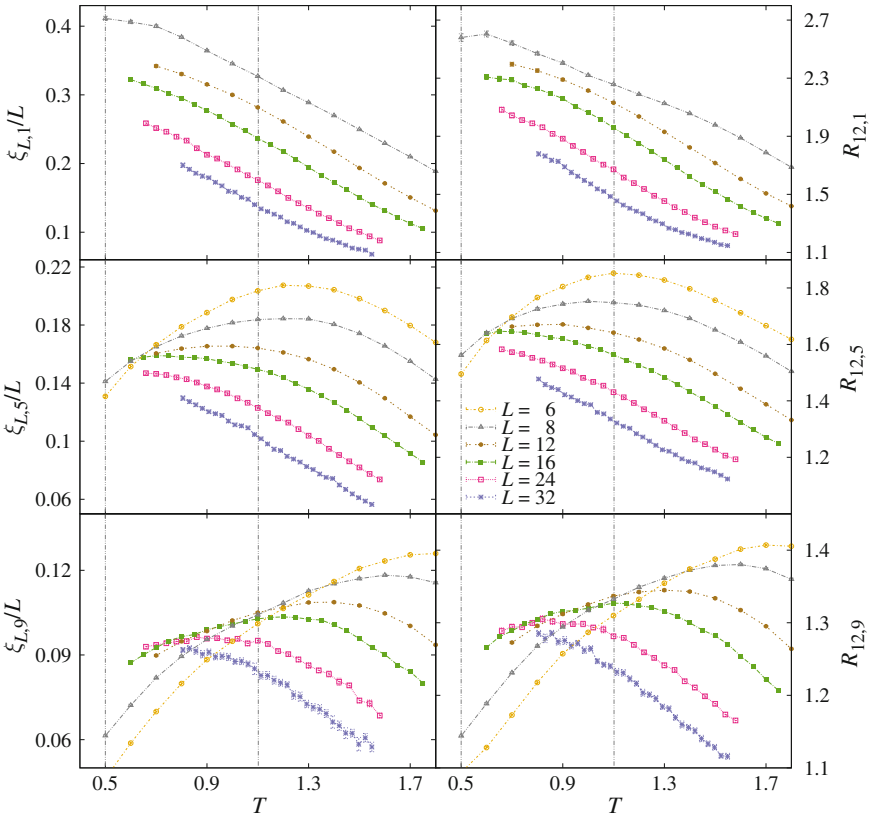

Fig. 2.13 Finite-size indicators of a phase transition, computed for $h = 0.2$. On the *left* side we plot, for quantiles 1 (*top*), 5 (*middle*) and 9 (*bottom*), the correlation length in units of the lattice size ξ_L/L (*left*) versus the temperature, for all our lattice sizes except $L = 6$ (we show in Sect. 2.7 that the quantile description is not suitable for $L = 6$ because there is a double peak in the $P(q)$). On the *right* we show analogous plots for R_{12} [defined in Eq. (1.46)]. The vertical line on the left marks the upper bound $T^{\rm up}$ for a possible phase transition given in [BJ14b], while the one on the right marks the zero-field transition temperature $T_{\rm c}$ given in [BJ13]. Quantile 1 has the same qualitative behavior of the average ξ_L/L, shown in Fig. 2.1, while quantiles 5 and 9 suggest a scale invariance at some temperature $T_h < T^{\rm up}$

that the 5th quantile is a better indicator, since the position of the fifth quantile $\tilde{q}_5$ has less finite-size effects (it practically has none, Fig. 2.9–inset) than $\tilde{q}_9$.

It is interesting to focus on the height of the crossings of each quantile from Fig. 2.13, and compare them with $h = 0.2$ (Fig. 2.13). This is expected to be a universal quantity, and in the hypothesis of a phase transition it should be the same for both fields. Although it is not possible to assign error bars to the these values, it is possible to see that both for $h = 0.1$ and $h = 0.2$ the heights are similar ($\xi_{L,5}/L \approx 0.15$, $\xi_{L,9}/L \approx 0.09$, $R_{12,5} \approx 1.6$, $R_{12,9} \approx 1.3$).

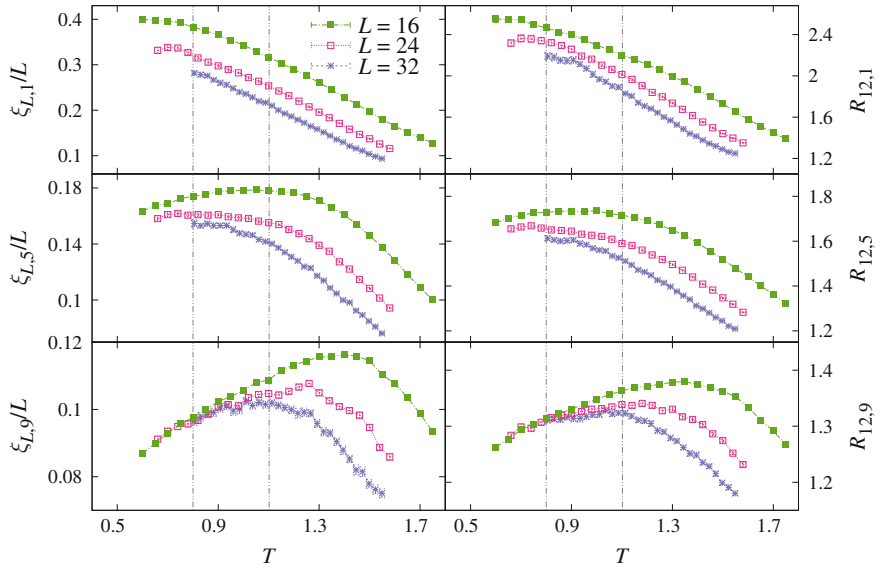

Fig. 2.14 Same as Fig. 2.13, but for $h = 0.1$. This time the effects of the zero-temperature transition are stronger, so we removed from the plot sizes $L = 6, 8, 12$. In Sect. 2.7 we show that the quantile description is not suitable for smaller lattices due to crossover effects from the zero-field behavior.

2.10 This is not an Echo of the $h = 0$ Transition

The crossing suggested by the quantiles 5 and 9 in Fig. 2.13 is unlikely to be caused by the zero-field transition, since it appears at $T < T_c$, and shifts towards lower temperatures as the lattice size increases. Also, the value of ξ_L/L (R_{12}) at the possible crossing point of the fifth quantile is upper-bounded to $\xi_L/L \simeq 0.16$ ($R_{12} \simeq 1.65$), while for $h = 0$ it is considerably larger ($\xi_L(T_c)/L \simeq 0.28$ [$R_{12}(T_c) \simeq 2.15$]), recall Sect. 2.6. In this section, we will advance more arguments contradicting the notion that what was seen resulted from the effects of zero-field transition.

2.10.1 An Escaping Transition

As pointed out in Sect. 2.3, there is a controversy because we observe a wide $P(q)$, just like in the mean-field model, but the curves $\xi_L/L(T)$ and $R_{12}(T)$ do not show any sign of a crossing. If we were in the presence of a phase transition, a straightforward explanation could reside in an anomalous exponent η close to 2 [BJ14d], since at the critical temperature the replicon susceptibility scales as $\chi_R(L) \sim L^{2-\eta}$ (1.91). It is possible to calculate η with the quotients' method [Nig75, Bal96], by comparing the susceptibility χ_L of different lattice sizes at the critical point T_c:

$$\frac{\chi_{2L}(T_c)}{\chi_L(T_c)} = 2^{2-\eta} + \cdots, \tag{2.19}$$

where the dots stand for subleading terms. This definition only makes sense at criticality, but we can extend it in an effective manner to a generic temperature. This way we can delineate an effective exponent

$$\eta_{\text{eff}}(T; L, 2L) = 2 - \log_2 \frac{\chi_{2L}(T)}{\chi_L(T)}. \tag{2.20}$$

In case there were a phase transition at a finite temperature T_h, we would have $\eta_{\text{eff}}(T_h) = \eta$. We should have $\eta_{\text{eff}} = 2$ in the paramagnetic phase, $\eta_{\text{eff}} = -1$ in the deep spin-glass phase[8] and signs of a crossing at $\eta_{\text{eff}} = \eta(h = 0) = -0.3900(36)$ [BJ13] in the limit of a complete domination by the $h = 0$ transition.

In Fig. 2.15 we show $\eta_{\text{eff}}(T)$ for $h = 0.4$, $h = 0.1$, and $h = 0$ (the $h = 0$ data come from the simulations we performed in [BJ13]).[9] If a phase transition were present, but hidden by heavy finite-size effects, we would expect at least that the L-trend of η_{eff} be decreasing. Contrarily, the larger our lattices, the wider the temperature range in which $\eta_{\text{eff}} = 2$. The apparent phase transition shifts towards lower temperature when we suppress finite-size effects. The data in our possession is not enough to state whether this shift will converge to a positive temperature. In any case, this is compatible with the upper bounds to a possible transition given in [BJ14b].

On the other side, η_{eff} stays positive for all our simulated lattices (except $h = 0.05$, $L = 6$), and that even for $T < T_c(h = 0)$ it tends to some value around 0.5, so it is unlikely that the null field transition is dominating the system's behavior.

2.10.2 Scaling at $T = T_c(h = 0)$

From the scaling with the lattice linear size of ξ_L/L at $T_c = T_c(h = 0)$, we can get another element to discard the hypothesis that the $h = 0$ transition is biasing significantly our measures. Assuming that there is no critical line for $h > 0$, a very large correlation length could be due to an echo of the zero-field transition or a low-temperature effect. In a theory that predicts that system is critical only at $h = 0$, $T = T_c$, the effects of this echo on the $h > 0$ behavior should be maximal near $T = T_c$. So, if we find a ξ that is large compared to our lattice sizes for $T < T_c$, a primary check is to monitor the scaling of the coherence length at T_c. Figure 2.16 shows the scaling of ξ_L/L at T_c with $h = 0.2$. We plot the average, the first, the fifth and the highest quantile. All of them show a clear decrease of ξ_L/L when increasing the lattice size, so our lattice sizes are large enough to state that the divergence at

[8] See Appendix B.21, keeping in mind that $\eta_{\text{eff}} = -1$ is somewhat trivial in the limit $h \to 0$, where χ reduces to $\chi = VE(q^2)$.

[9] For each jackknife block we calculated $\eta_{\text{eff}}(T)$ and made a cubic spline temperature interpolation.

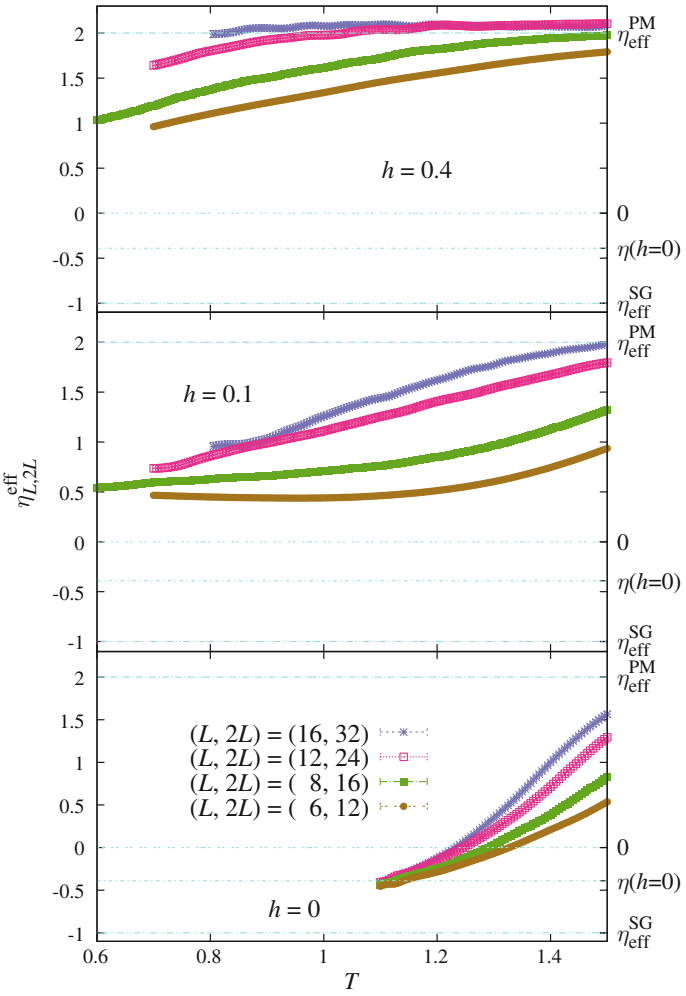

Fig. 2.15 We plot $\eta_{\rm eff}(T)$, defined in (2.20), for all the pairs $(L, 2L)$ we could form. The magnetic fields are $h = 0.4$ (*top*), $h = 0.1$ (*center*) and $h = 0$ (*bottom*). The $h = 0$ data comes from [BJ13]. In each plot we uses horizontal lines to underline meaningful limits, and we label them with a tic on the right axis. From up to down, we depict the limit $\eta^{\rm PM}_{\rm eff} = 2$ of a system in the paramagnetic phase, the $\eta_{\rm eff} = 0$ axis, the zero-field value $\eta_{\rm eff}(h = 0, T_{\rm c}) = -0.3900(36)$ [BJ13], and its value in a deep spin-glass phase $\eta^{\rm SG}_{\rm eff} = -1$. Notice the difference between the case with or without a field. For $h = 0.1$ the curves appear to converge to a positive $\eta_{\rm eff} \simeq 0.5$, while in the latter all the curves become negative and merge at $\eta_{\rm eff}(h = 0, T_{\rm c})$

$h = 0$ is not dominating ξ_L's behavior. On the other side, we are still far from the thermodynamic limit, since when the lattices are large enough, $\xi_L(T_{\rm c})/L$ should decay to zero linearly in $1/L$.

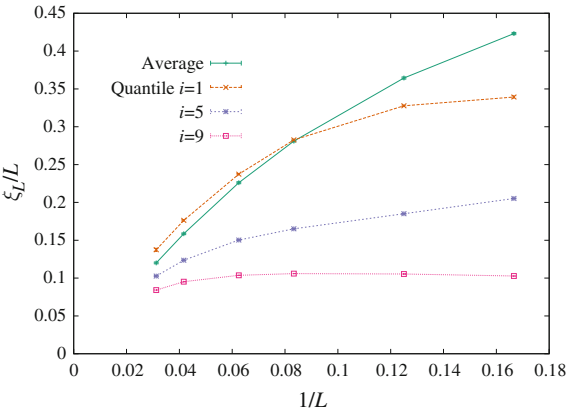

Fig. 2.16 Scaling of ξ_L/L at the null-field critical temperature $T_c = 1.109(29)$ [BJ13], with $h = 0.2$. We show the behavior of the average, and of quantiles 1, 5 and 9. If L is large enough, ξ_L/L should go as $1/L$, while if the system is seeing purely an echo of the divergence of the $h = 0$ transition transition, then ξ_L/L should be constant

2.11 Overview

We have studied the equilibrium behavior of the three-dimensional Ising Edwards–Anderson spin glass in an external magnetic field. Thermalizing the system at sufficiently low temperature was a computationally hard task and required the use of the JANUS dedicated computer to thermalize lattice sizes up to $L = 32$, down to temperatures $T \geq 0.8$.

First of all, we carried out a traditional analysis of our data. We chose observables that would be scale invariant at the critical temperature, and compared them for different lattice sizes, looking for crossings in their temperature curves. With this procedure we found no traces of a phase transition.

Yet, the scenario is more complicated. Despite the absence of crossings, indications that something non-trivial is going on are given by signals such as a growing correlation length (even for our largest lattices), peaks in the susceptibility, and a wide probability distribution function of the overlap.

We noticed a wide variety of behaviors within the same set of simulation parameters. Some measurements presented signs of criticality, while others did not. So, we tried to classify them in a meaningful way. We sorted our observables with the help of a CV, and came up with a quantitative criterion to select the best CV. Between the ones we proposed, the function of the instant overlaps that made the best CV turned out to be the median overlap q_{med}.

As a function of the median overlap, the scenario appeared rather non-trivial. The averages turned out to be dominated by a very small number of measurements. Those with a small q_{med} behaved similarly to the average: long correlation lengths, very large susceptibilities, and no signs of criticality. On the other side, the median behavior was far from the average, and the behavior of most of the measurements was qualitatively different from the average, with smaller correlation lengths and susceptibilities, but non-negligible indications of scale invariance right below the upper bound $T^{\text{up}}(h)$ given in [BJ14b]. Furthermore, separating the different behaviors of the system we

obtain mutually consistent indications of criticality from our primary dimensionless magnitudes $\xi_{L,i}/L$ and $R_{12,i}$. The achievement of this consistency is an important step forward with respect to [Bn12a], where the phase transition was revealed only by the R_{12} indicator, but it was invisible to ξ_L/L.

Unfortunately we were not able to make a quantitative prediction on the critical temperatures $T_c(h)$, because the observables as a function of the lattice size and of the temperature were very nonlinear, and the temperatures we reached were not low enough reliably to identify the crossing points of the quantile-dependent $\xi_{L,i}/L$ and $R_{12,i}$.

Overall, the presence of a phase transition appears plausible from our simulations. Perhaps more importantly, now the challenge is well defined: in order to be able to give, numerically, a conclusive answer on the presence of a de Almeida-Thouless line we need push our simulations down to $T \simeq 0.4$ (at $h = 0.2$). We believe that *Janus II*, the next generation of our dedicated computer [BJ14b], will be able to assume this challenge.

References

[AB10a] R. Alvarez Baños, A. Cruz, L.A. Fernandez, J.M. Gil-Narvion, A. Gordillo-Guerrero, M. Guidetti, A. Maiorano, F. Mantovani, E. Marinari, V. Martin-Mayor, J. Monforte-Garcia, A. Muñoz Sudupe, D. Navarro, G. Parisi, S. Perez-Gaviro, J.J. Ruiz-Lorenzo, S.F. Schifano, B. Seoane, A. Tarancon, R. Tripiccione and D. Yllanes (Janus Collaboration): J. Stat. Mech. **2010**, P06026 (2010). doi:10.1088/1742-5468/2010/06/P06026. arXiv:1003.2569

[AB10b] R. Alvarez Baños, A. Cruz, L. A. Fernandez, J.M. Gil-Narvion, A. Gordillo-Guerrero, M. Guidetti, A. Maiorano, F. Mantovani, E. Marinari, V. Martin-Mayor, J. Monforte-Garcia, A. Muñoz Sudupe, D. Navarro, G. Parisi, S. Perez-Gaviro, J.J. Ruiz-Lorenzo, S.F. Schifano, B. Seoane, A. Tarancon, R. Tripiccione, D. Yllanes (Janus Collaboration): Phys. Rev. Lett. **105**, 177202 (2010). doi:10.1103/PhysRevLett.105.177202. arXiv:1003.2943

[BJ12] M. Baity-Jesi, R. A. Baños, A. Cruz, L.A. Fernandez, J.M. Gil-Narvion, A. Gordillo-Guerrero, M. Guidetti, D. Iniguez, A. Maiorano, F. Mantovani, E. Marinari, V. Martin-Mayor, J. Monforte-Garcia, A. Munoz Sudupe, D. Navarro, G. Parisi, M. Pivanti, S. Perez-Gaviro, F. Ricci-Tersenghi, J.J. Ruiz-Lorenzo, S.F. Schifano, B. Seoane, A. Tarancon, P. Tellez, R. Tripiccione, D. Yllanes, Eur. Phys. J. Special Topics **210**, 33 (2012). doi:10.1140/epjst/e2012-01636-9. arXiv:1204.4134

[BJ13] M. Baity-Jesi, R.A. Baños, A. Cruz, L.A. Fernandez, J.M. Gil-Narvion, A. Gordillo-Guerrero, D. Iniguez, A. Maiorano, F. Mantovani, E. Marinari, V. Martin-Mayor, J. Monforte-Garcia, A. Muñoz, Sudupe, D. Navarro, G. Parisi, S. Perez-Gaviro, M. Pivanti, F. Ricci-Tersenghi, J.J. Ruiz-Lorenzo, S.F. Schifano, B. Seoane, A. Tarancon, R. Tripiccione, D. Yllanes (Janus Collaboration). Phys. Rev. B **88**, 224416 (2013). doi:10.1103/PhysRevB.88.224416. arXiv:1310.2910

[BJ14a] M. Baity-Jesi, R.A. Baños, A. Cruz, L.A. Fernandez, J.M. Gil-Narvion, A. Gordillo-Guerrero, D. Iniguez, A. Maiorano, M.F., E. Marinari, V. Martin-Mayor, J. Monforte-Garcia, A. Muñoz Sudupe, D. Navarro, G. Parisi, S. Perez-Gaviro, M. Pivanti, F. Ricci-Tersenghi, J.J. Ruiz-Lorenzo, S.F. Schifano, B. Seoane, A. Tarancon, R. Tripiccione, D. Yllanes, J. Stat. Mech. **2014**, P05014 (2014). doi:10.1088/1742-5468/2014/05/P05014. arXiv:1403.2622

[BJ14b] M. Baity-Jesi, R.A. Baños, A. Cruz, L.A. Fernandez, J.M. Gil-Narvion, A. Gordillo-Guerrero, D. Iniguez, A. Maiorano, M. F., E. Marinari, V. Martin-Mayor, J. Monforte-Garcia, A. Muñoz Sudupe, D. Navarro, G. Parisi, S. Perez-Gaviro, M. Pivanti, F. Ricci-Tersenghi, J.J. Ruiz-Lorenzo, S.F. Schifano, B. Seoane, A. Tarancon, R. Tripiccione, D. Yllanes, Phys. Rev. E **89**, 032140 (2014). doi:10.1103/PhysRevE.89.032140. arXiv:1307.4998

[BJ14d] M. Baity-Jesi, L.A. Fernandez, V. Martin-Mayor, J.M. Sanz, Phys. Rev. **89**, 014202 (2014). doi:10.1103/PhysRevB.89.014202. arXiv:1309.1599

[Bal00] H.G. Ballesteros, A. Cruz, L.A. Fernandez, V. Martin-Mayor, J. Pech, J.J. Ruiz-Lorenzo, A. Tarancon, P. Tellez, C.L. Ullod, C. Ungil, Phys. Rev. B **62**, 14237–14245 (2000). doi:10.1103/PhysRevB.62.14237. arXiv:cond-mat/0006211

[Bal96] H.G. Ballesteros, L.A. Fernandez, V. Martin-Mayor, A. Muñoz, Sudupe. Phys. Lett. B **378**, 207 (1996). doi:10.1016/0370-2693(96)00358-9. arXiv:hep-lat/9511003

[Bn11] R.A. Baños, A. Cruz, L.A. Fernandez, J.M. Gil-Narvion, A. Gordillo-Guerrero, M. Guidetti, D. Iñiguez, A. Maiorano, F. Mantovani, E. Marinari, V. Martin-Mayor, J. Monforte-Garcia, A. Muñoz Sudupe, D. Navarro, G. Parisi, S. Perez-Gaviro, F. Ricci-Tersenghi, J.J. Ruiz-Lorenzo, S.F. Schifano, B. Seoane, A. Tarancón, R. Tripiccione, D. Yllanes, Phys. Rev. B **84**, 174209 (Nov 2011). doi:10.1103/PhysRevB.84.174209. arXiv:1107.5772, http://link.aps.org/doi/10.1103/PhysRevB.84.174209

[Bn12a] R.A. Baños, A. Cruz, L.A. Fernandez, J.M. Gil-Narvion, A. Gordillo-Guerrero, M. Guidetti, D. Iniguez, A. Maiorano, E. Marinari, V. Martin-Mayor, J. Monforte-Garcia, A. Muñoz, Sudupe, D. Navarro, G. Parisi, S. Perez-Gaviro, J.J. Ruiz-Lorenzo, S.F. Schifano, B. Seoane, A. Tarancon, P. Tellez, R. Tripiccione, D. Yllanes, Proc. Natl. Acad. Sci. USA **109**, 6452 (2012). doi:10.1073/pnas.1203295109

[Bel08a] F. Belletti, M. Cotallo, A. Cruz, L.A. Fernandez, A. Gordillo, A. Maiorano, F. Mantovani, E. Marinari, V. Martin-Mayor, A. Muñoz Sudupe, D. Navarro, S. Perez-Gaviro, J.J. Ruiz-Lorenzo, S.F. Schifano, D. Sciretti, A. Tarancon, R. Tripiccione, J.L. Velasco (Janus Collaboration): Comp. Phys. Comm. **178**, 208–216 (2008). doi:10.1016/j.cpc.2007.09.006. arXiv:0704.3573

[Bel09a] F. Belletti, A. Cruz, L.A. Fernandez, A. Gordillo-Guerrero, M. Guidetti, A. Maiorano, F. Mantovani, E. Marinari, V. Martin-Mayor, J. Monforte, A. Muñoz, Sudupe, D. Navarro, G. Parisi, S. Perez-Gaviro, J.J. Ruiz-Lorenzo, S.F. Schifano, D. Sciretti, A. Tarancon, R. Tripiccione, D. Yllanes (Janus Collaboration). J. Stat. Phys. **135**, 1121 (2009). doi:10.1007/s10955-009-9727-z. arXiv:0811.2864

[Bel06] F. Belletti, F. Mantovani, G. Poli, S.F. Schifano, R. Tripiccione, I. Campos, A. Cruz, D. Navarro, S. Perez-Gaviro, D. Sciretti, A. Tarancon, J.L. Velasco, P. Tellez, L.A. Fernandez, V. Martin-Mayor, A. Muñoz, Sudupe, S. Jimenez, A. Maiorano, E. Marinari, J.J. Ruiz-Lorenzo (Janus Collaboration). Comput. Sci. Eng. **8**, 41 (2006)

[Bel09b] F. Belletti, M. Guidetti, A. Maiorano, F. Mantovani, S.F. Schifano, R. Tripiccione, M. Cotallo, S. Perez-Gaviro, D. Sciretti, J.L. Velasco, A. Cruz, D. Navarro, A. Tarancon, L.A. Fernandez, V. Martin-Mayor, A. Muñoz-Sudupe, D. Yllanes, A. Gordillo-Guerrero, J.J. Ruiz-Lorenzo, E. Marinari, G. Parisi, M. Rossi, G. Zanier, Janus collaboration. Comput. Sci. Eng. **11**, 48 (2009). doi:10.1109/MCSE.2009.11

[Bra80b] A.J. Bray, M.A. Moore, J. Phys. C: Solid St. Phys. **13**, 419 (1980). doi:10.1088/0022-3719/13/3/016

[Cas05] T. Castellani, A. Cavagna, J. Stat. Mech. **2005**, P05012 (2005). doi:10.1088/1742-5468/2005/05/P05012

[Cav09] A. Cavagna, Phys. Rep. **476**, 51–124 (2009). arXiv:0903.4264

[Deb97] P.G. Debenedetti, *Metastable Liquids* (Princeton University Press, Princeton, 1997)

[Deb01] P.G. Debenedetti, F.H. Stillinger, Nature **410**, 259–267 (2001)

[Fer09a] L.A. Fernandez, V. Martin-Mayor, Phys. Rev. E **79**, 051109 (2009). doi:10.1103/PhysRevE.79.051109

[Fer13] L.A. Fernandez, V. Martin-Mayor, G. Parisi, B. Seoane, EPL **103**, 67003 (2013). doi:10.1209/0295-5075/103/67003. arXiv:1307.2361

[Fer09b] L.A. Fernandez, V. Martin-Mayor, S. Perez-Gaviro, A. Tarancon, A.P. Young, Phys. Rev. B **80**, 024422 (2009). doi:10.1103/PhysRevB.80.024422
[Ful13] C.J. Fullerton, M.A. Moore (2013). arXiv:1304.4420
[Gun91] K. Gunnarsson, P. Svedlindh, P. Nordblad, L. Lundgren, H. Aruga, A. Ito, Phys. Rev. B **43**, 8199–8203 (1991). doi:10.1103/PhysRevB.43.8199
[Huk96] K. Hukushima, K. Nemoto, J. Phys. Soc. Japan **65**, 1604 (1996). doi:10.1143/JPSJ.65.1604. arXiv:cond-mat/9512035
[Hyn96] R. Hyndman, Y. Fan, Am. Stat. **50**, 361 (1996)
[Jön05] P.E. Jönsson, H. Takayama, H.A. Katori, A. Ito, Phys. Rev. B **71**, 180412(R) (2005). doi:10.1103/PhysRevB.71.180412. arXiv:cond-mat/0411291
[Jör08b] T. Jörg, H.G. Katzgraber, F. Krzakala, Phys. Rev. Lett. **100**, 197202 (2008). doi:10.1103/PhysRevLett.100.197202. arXiv:0712.2009
[Kir87] T.R. Kirkpatrick, D. Thirumalai, Phys. Rev. B **36**, 5388 (1987). doi:10.1103/PhysRevB.36.5388
[Kir89] T.R. Kirkpatrick, D. Thirumalai, P.G. Wolynes, Phys. Rev. A **40**, 1045 (1989)
[Kot83] G. Kotliar, P.W. Anderson, D.L. Stein, Phys. Rev. B **27**, 602 (1983). doi:10.1103/PhysRevB.27.602
[Lar13] D. Larson, H.G. Katzgraber, M.A. Moore, A.P. Young, Phys. Rev. B **87**, 024414 (2013). doi:10.1103/PhysRevB.87.024414. arXiv:1211.7297
[Leu13] L. Leuzzi, G. Parisi, Phys. Rev. B **88**, 224204 (2013). arXiv:1303.6333
[Leu08] L. Leuzzi, G. Parisi, F. Ricci-Tersenghi, J.J. Ruiz-Lorenzo, Phys. Rev. Lett. **101**, 107203 (2008). doi:10.1103/PhysRevLett.101.107203
[Mar98] E. Marinari, *In Advances in Computer Simulation*, ed. by J. Kondor (Springer-Verlag, Kerstész and I, 1998)
[Moo02] M.A. Moore, B. Drossel, Phys. Rev. Lett. **89**, 217202 (2002). doi:10.1103/PhysRevLett.89.217202. arXiv:cond-mat/0201107
[New99] M.E.J. Newman, G.T. Barkema, *Monte Carlo Methods in Statistical Physics* (Clarendon Press, Oxford, 1999)
[Nig75] M.P. Nightingale, Physica A **83**, 561 (1975). doi:10.1016/0378-4371(75)90021-7
[Pal99a] M. Palassini, S. Caracciolo, Phys. Rev. Lett. **82**, 5128–5131 (1999). doi:10.1103/PhysRevLett.82.5128. arXiv:cond-mat/9904246
[Par12a] G. Parisi, F. Ricci-Tersenghi, Phil. Mag. **92**, 341 (2012). doi:10.1080/14786435.2011.634843. arXiv:1108.0759v1
[Par12b] G. Parisi, T. Temesvári, Nucl. Phys. B **858**, 293 (2012). arXiv:1111.3313
[Pet99] D. Petit, L. Fruchter, I.A. Campbell, Phys. Rev. Lett. **83**, 5130 (1999). doi:10.1103/PhysRevLett.83.5130. arXiv:cond-mat/9910353
[Pet02] D. Petit, L. Fruchter, I.A. Campbell, Phys. Rev. Lett. **88**, 207206 (2002). doi:10.1103/PhysRevLett.88.207206. arXiv:cond-mat/011112
[Seo13] B. Seoane: *Spin glasses, the quantum annealing, colloidal glasses and crystals: exploring complex free-energy landscapes*. Ph.D. thesis, Universidad Complutense de Madrid (January 2013)
[Tab10] Y. Tabata, K. Matsuda, S. Kanada, T. Yamazaki, T. Waki, H. Nakamura, K. Sato, K. Kindo, J. Phys. Soc. Japan. **79**, 123704 (2010). arXiv:1009.6115
[Tem08] T. Temesvári, Phys. Rev. B **78**, 220401 (2008)
[Tem02] T. Temesvári, C. De Dominicis, Phys. Rev. Lett. **89**, 097204 (2002). doi:10.1103/PhysRevLett.89.097204. arXiv:cond-mat/0207512
[Yll11] D. Yllanes, *Rugged Free-Energy Landscapes in Disordered Spin Systems*. Ph.D. thesis, Universidad Complutense de Madrid (2011). arXiv:1111.0266
[You04] A.P. Young, H.G. Katzgraber, Phys. Rev. Lett. **93**, 207203 (2004). doi:10.1103/PhysRevLett.93.207203. arXiv:cond-mat/0407031

http://www.springer.com/978-3-319-41230-6

Spin Glasses
Criticality and Energy Landscapes
Baity Jesi, M.
2016, XXIX, 221 p. 71 illus., 24 illus. in color., Hardcover
ISBN: 978-3-319-41230-6